Hindawi
Mathematical Problems in Engineering
Volume 2019, Article ID 5084098, 14 pages
https://doi.org/10.1155/2019/5084098

Research Article

Continuum Analysis of Rarefaction Effects on a Thermally Induced Gas Flow

Mohamed Hssikou,[1] **Jamal Baliti**,[2] **and Mohammed Alaoui**[3]

[1]*Faculty of Sciences, Ibn Zohr University, Agadir, Morocco*
[2]*Polydisciplinary Faculty, Sultan Moulay Slimane University, Beni Mellal, Morocco*
[3]*Faculty of Sciences, Moulay Ismaïl University, Meknes, Morocco*

Correspondence should be addressed to Mohamed Hssikou; hssikoumed@gmail.com

Received 8 January 2019; Accepted 7 April 2019; Published 30 April 2019

Academic Editor: Hang Xu

A Maxwell gas confined within a micro cavity with nonisothermal walls is investigated in the slip and early transition regimes using the classical and extended continuum theories. The vertical sides of the cavity are kept at the uniform and environmental temperature T_0, while the upper and bottom ones are linearly heated in opposite directions from the cold value T_0 to the hot one T_H. The gas flow is, therefore, induced only by the temperature gradient created along the longitudinal walls. The problem is treated from a macroscopic point of view by solving numerically the so-called regularized 13-moment equations (R13) recently developed as an extension of Grad 13-moment theory to the third order of the Knudsen number powers in the Chapman-Enskog expansion. The gas macroscopic properties obtained by this method are compared with the classical continuum theory results (NSF) using the first and second order of velocity slip and temperature jump boundary conditions. The gas flow behavior is studied as a function of the Knudsen number (Kn), nonlinear effects, for different heating rates T_0/T_H. The micro cavity aspect ratio effect is also evaluated on the flow fields in this study.

1. Introduction

The frequent use of small-size devices in several applications needs types of equipment that dissipate maximum amount of heat per unit area. With the development of micro-electro-mechanical systems (MEMS), the heat transfer mechanism has gained recently a great interest. The micro pumps, micro ducts, micro nozzles, micro turbines, and micro valves are some typical examples of these small devices involving liquid and gas flows [1–3]. Regarding the dimensions of these devices, the continuum assumptions of the gas flow break down and some deviations are observed in respect of the macro scale case. The use of velocity slip and temperature jump boundary conditions proves that the rarefaction degree has a significant effect on the gas micro flows or low-pressure gas problems (Karniadakis and Beskok 2005, [4]). To estimate the degree of rarefaction, the so-called Knudsen number defined as $Kn \sim \lambda/L$ is used to classify the flow regimes, where λ and L represent, respectively, the mean free path and a characteristic length of the system. For $Kn < 10^{-3}$ the flow can be considered as a continuum medium; hence the classical Navier-Stokes and Fourier equations are sufficient to describe the gas flow behavior. In the range of $10^{-3} \leq Kn < 0.1$ (slip regime), the gas flow fields can be described using these equations if the typical boundary conditions of velocity slip and temperature jump are applied at the walls [5]. After the slip limit, $0.1 \leq Kn < 10$, i.e., transition regime, the nonequilibrium effects become more important even in the bulk of flow and, therefore, the continuum theory breaks down [6, 7]. In this case, the gas flow must be described from a kinetic point of view by following the governing equation of Boltzmann (3). However, the high-dimensionality of this equation makes its direct solving extremely expensive in the discrete phase space. So far, the direct simulation Monte Carlo (DSMC) method is the main practical method used to characterize the strong nonequilibrium flows in NEMS/MEMS [8, 9]. However, the DSMC method is very expensive both in computational time

and memory requirements, especially for low-speed flow in microelectromechanical devices (MEMS) and nanodevices [10]. In thermal cavities, when Kn number increases, the intermolecular- and molecular-surface interactions decrease [11]. Therefore, a huge number of particles are needed to capture the flow features. In the macroscopic point of view, the problems involving Couette and Fourier flows have been treated enough with isothermal walls in the previous study [12–15]. However, minor attempts have been observed for treating the problems with nonisothermal walls boundary conditions [16–18]. In this case, a thermal slip gas flow is induced under the effects of *transpiration* or *thermal creep* flows; i.e., the gas is forced into motion at the boundaries. The thermal creep flow of a rarefied gas within an enclosure is treated deterministically by solving, on the one hand, the Boltzmann-Shakhov model equation and using DSMC as a stochastic approach in the range of $10^{-2} < Kn < 10$ [17]. On the other hand, in such problem, a competition between thermal creep flow and thermal stress flow induced by a gradient of heat flux in the bulk is investigated as a function of rarefaction degree (Kn) [19]. At the micro scale and rarefied conditions, the temperature inhomogeneity of a gas system can lead to a variety of flow phenomena such as the *ghost effects* observed at the continuum limit [20]. The fact that many of these micro devices involve slip and early transition regime gas flows is the first motivation of this continuum study. The second one is to evaluate the *thermal slip* contribution in the velocity slip and temperature jump phenomena near the heated walls, which is proportional to the tangential temperature gradient [21]. This effect is the main correction made by the second order of velocity slip and temperature jump in the NSF approach. Investigating thermal behaviors under rarefied condition due to high power densities requires the application of efficient techniques to predict allowable performance limits of these systems [22]. By comparing the DSMC method and R13 solution, it is shown that the R13 equations can be solved in short computation time as compared to those for DSMC method [23]. Thus, the main goal of this paper is to investigate the rarefaction effects on the macroscopic proprieties of a dilute gas flow induced only by nonisothermal walls effects, thermal creep flow, using the classical and extended continuum-based model. The regularized 13-moment equations (R13), developed by [24], are solved numerically to capture the strong rarefaction or nonlinear effects that occur in the early transition regime. In this study, we discuss also the validity of the first (NSF1) and second (NSF2) orders of velocity slip and temperature jump boundary conditions in the Navier-Stokes and Fourier solution, within the rarefaction range of $0.05 \leq Kn \leq 0.3$. In this study, we assume that the gas is not subjected to any external body force. In the next section, we present a brief description of the problem, after we recall the set of basic equations and the boundary conditions used in both solutions of NSF and R13.

2. Statement of Problem

A Maxwell and monatomic gas is confined within a two-dimensional heated microcavity with orthogonal cross section of $H \times L$ being shown in Figure 1. The left and right walls of the cavity are kept at a uniform and environmental temperature $T_0 = 273K$ while the bottom and upper sides are linearly heated from the cold value T_0 to hot one T_H in opposite directions; i.e., $T(x)|_{y=0,H} = T_{0,H} \pm (T_H - T_0)x/L$. The macroscopic properties of the gas are evaluated for different values of Knudsen number in the slip and early transition regimes for the hot temperatures $1.25T_0$,$1.5T_0$, $1.75T_0$, and $2T_0$. Two values of the cavity aspect ratio, $AR = H/L$, are considered in this study ($AR = 2$ and 1). Figure 1 shows the configuration of the cavity in a square geometry ($AR = 1$). The flow fields are evaluated as a function of Knudsen number Kn defined as

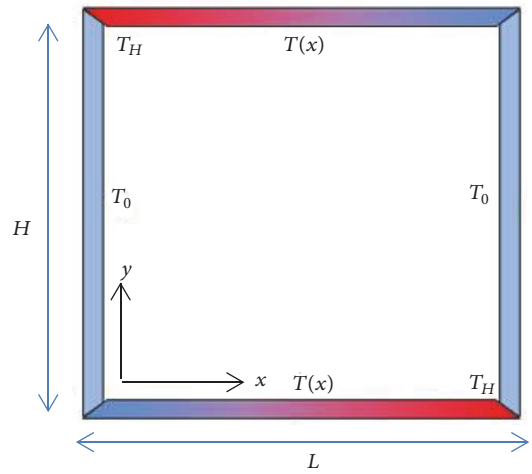

Figure 1: Micro cavity geometry.

$$Kn = \frac{\mu_0 v_0}{p_0} \frac{1}{L} \tag{1}$$

where R, μ_0, and p_0 denote, respectively, the gas specific constant, the reference viscosity at the temperature T_0, and the hydrostatic pressure given by $p_0 = \rho_0 R T_0$. Also $v_0 = \sqrt{2RT_0}$ is the most probable molecular velocity which is taken as the characteristic velocity.

3. Continuum Model Based Description

The evolution equations for density, velocity, and internal energy ε are given by the conservation laws of mass, momentum, and energy that can be written in the general form as follows:

$$\frac{\partial \rho}{\partial t} + \frac{\partial \rho v_i}{\partial x_i} = 0, \tag{2a}$$

$$\frac{\partial \rho v_i}{\partial t} + \frac{\partial \left(P_{ik} + \rho v_i v_k\right)}{\partial x_k} = 0, \tag{2b}$$

$$\frac{\partial \rho \left(\varepsilon + (1/2)\, v^2\right)}{\partial t} + \frac{\partial \left(\rho \left(\varepsilon + (1/2)\, v^2\right) v_k + P_{ik} v_i + q_k\right)}{\partial x_k} = 0, \tag{2c}$$

where ρ, v_k, P_{ik}, and q_k denote, respectively, mass density, macroscopic velocity, pressure tensor, and heat flux vector components. Note that the pressure tensor is related to the hydrostatic pressure and stress tensor by the relation: $P_{ij} = p\delta_{ij} + \sigma_{ij}$ where δ_{ij} represents the Kronecker delta. In the frame of ideal gas approximation, the hydrostatic pressure is given by $p = \rho RT = \rho\theta$ where θ corresponds to the temperature in energy units. To close this set of equations, one needs to define the constitutive equations including the relationship between the stress tensor $\boldsymbol{\sigma}$, the heat flux vector $\mathbf{q}$, and the macroscopic variables derivatives. As an extension of the classical NSF theory, Grad introduces the balance equations corresponding to higher order moments of the particle velocity distribution function $f(\mathbf{r}, \mathbf{c}, t)$ [26] in which the evolution is governed by the Boltzmann equation given by

$$\left(\frac{\partial}{\partial t} + \mathbf{c}.\nabla_{\mathrm{r}}\right) f = J\left[f, f'\right], \tag{3}$$

where $J[f, f']$ and $\mathbf{c}$ are, respectively, the collisions operator and the molecular velocity.

Due to the collision's random nature, the exact analytic solution of (3) remains difficult. For this reason, some approximations are used to simplify this term for the small deviations in respect of the equilibrium state. In this context, it has been shown recently that the Grad's approach accuracy can be further improved up to $\mathcal{O}(Kn^3)$ of the Knudsen number powers in the Chapman-Enskog expansion by regularization of the moment equations of Grad [27, 28]. Note that the NSF solution with velocity slip and temperature jump boundary conditions leads to the first order in this expansion.

In the 13-moment theory of Grad, the gas state is described by the set of 13 moments of functions $\varphi_A = m\{1, c_i, (1/2)C^2, C_{\langle i}C_{j\rangle}, (1/2)C^2C_i\}$. The Multiplication of (3), at the steady state, by φ_A and subsequently by integration over velocity space yields the governing equations of moments: mass density, hydrodynamic (bulk) velocity, hydrostatic pressure, stress tensor, temperature, and heat flux vector related to the distribution function by

$$\rho(x, y) = m\int f(\mathbf{r}, \mathbf{c})\, \mathrm{d}\mathbf{c}, \tag{4}$$

$$\mathbf{v}(x, y) = \frac{m}{\rho(x, y)}\int \mathbf{c} f(\mathbf{r}, \mathbf{c})\, d\mathbf{c}, \tag{5}$$

$$p(x, y) = \frac{m}{3}\int C^2 f(\mathbf{r}, \mathbf{c})\, d\mathbf{c}, \tag{6}$$

$$P_{ij}(x, y) = m\int C_{\langle i}C_{j\rangle} f(\mathbf{r}, \mathbf{c})\, d\mathbf{c}, \tag{7}$$

$$T(x, y) = \frac{m}{3nK_B}\int C^2 f(\mathbf{r}, \mathbf{c})\, d\mathbf{c}, \tag{8}$$

$$\mathbf{q}(x, y) = \frac{m}{2}\int C^2\mathbf{C} f(\mathbf{r}, \mathbf{c})\, d\mathbf{c} \tag{9}$$

where $\mathbf{C} = \mathbf{c} - \mathbf{v}$ is the peculiar velocity.

By setting $\varphi_A = m, mc_i$ and $(1/2)mC^2$, respectively, and using the invariance property of the collisions operator, the right side of (3), one can find the balance equations ((2a), (2b), (2c)). The two other values of φ_A lead to the nonlinear constitutive equations of stress tensor σ_{ij} and heat flux vector q_i, respectively, that are given in the so-called R13 approach by [27]

$$\begin{aligned}&\frac{\partial\sigma_{ij}}{\partial t} + \frac{\partial\sigma_{ij}v_k}{\partial x_k} + \frac{4}{5}\frac{\partial q_{\langle i}}{\partial x_{j\rangle}} + 2p\frac{\partial v_{\langle i}}{\partial x_{j\rangle}} + 2\sigma_{k\langle i}\frac{\partial v_{j\rangle}}{\partial x_k}\\ &\quad + \frac{\partial m_{ijk}}{\partial x_k} = -\frac{p}{\mu}\sigma_{ij},\end{aligned} \tag{10}$$

$$\begin{aligned}&\frac{\partial q_i}{\partial t} + \frac{\partial q_i v_k}{\partial x_k} + \frac{5}{2}p\frac{\partial\theta}{\partial x_i} + \frac{5}{2}\sigma_{ik}\frac{\partial\theta}{\partial x_k} + \theta\frac{\partial\sigma_{ik}}{\partial x_k}\\ &\quad - \sigma_{ik}\frac{\theta}{\rho}\frac{\partial\rho}{\partial x_k} - \frac{\sigma_{ik}}{\rho}\frac{\partial\sigma_{kl}}{\partial x_l} + \frac{7}{5}q_k\frac{\partial v_i}{\partial x_k} + \frac{2}{5}q_k\frac{\partial v_k}{\partial x_i}\\ &\quad + \frac{2}{5}q_i\frac{\partial v_k}{\partial x_k} + \frac{1}{2}\frac{\partial R_{ik}}{\partial x_k} + \frac{1}{6}\frac{\partial\Delta}{\partial x_i} + m_{ikl}\frac{\partial v_k}{\partial x_l} = -\frac{2}{3}\frac{p}{\mu}q_i,\end{aligned} \tag{11}$$

where the indices in the angular brackets denote the symmetric trace-free parts of tensors. The R13 equations closure contains, therefore, additional quantities m_{ijk}, R_{ik}, and Δ, corresponding to the higher order moments, given by [24, 28, 29]

$$\begin{aligned}\Delta &= -\frac{\sigma_{kl}\sigma_{kl}}{\rho} + 6\frac{\sigma_{kl}\sigma_{kl}^{NSF}}{\rho} + \frac{56}{6}\frac{q_k q_k^{NSF}}{p}\\ &\quad - 12\frac{\mu}{p}\left(\theta\frac{\partial q_k}{\partial x_k} - \theta q_k\frac{\partial\ln p}{\partial x_k}\right),\end{aligned} \tag{12a}$$

$$\begin{aligned}R_{ij} &= -\frac{4}{7}\frac{\sigma_{k\langle i}\sigma_{j\rangle k}}{\rho} + \frac{24}{7}\frac{\sigma_{k\langle i}\sigma_{j\rangle k}^{NSF}}{\rho} + \frac{192}{75}\frac{q_{\langle i}q_{j\rangle}^{NSF}}{p}\\ &\quad - \frac{24}{5}\frac{\mu}{p}\left(\theta\frac{\partial q_{\langle i}}{\partial x_{j\rangle}} - \theta q_{\langle i}\frac{\partial\ln p}{\partial x_{j\rangle}}\right),\end{aligned} \tag{12b}$$

$$\begin{aligned}m_{ijk} &= \frac{8}{15}\frac{\sigma_{\langle ij}q_{k\rangle}^{NSF}}{p} + \frac{4}{5}\frac{q_{\langle i}\sigma_{jk\rangle}^{NSF}}{p}\\ &\quad - 2\frac{\mu}{p}\left(\theta\frac{\partial\sigma_{\langle ij}}{\partial x_{k\rangle}} - \theta\sigma_{\langle ij}\frac{\partial\ln p}{\partial x_{k\rangle}}\right).\end{aligned} \tag{12c}$$

If one neglects these quantities, the R13 set of equations will be reduced to the well-known set of Grad's 13-moment equations. At the small values of Kn ($Kn << 1$), the stress tensors and heat flux components can be written in the Chapman-Enskog expansion of Knudsen number powers as follows.

$$\sigma_{ij} = \sigma_{ij}^{(0)} + Kn\sigma_{ij}^{(1)} + Kn^2\sigma_{ij}^{(2)}\ldots \tag{13}$$

$$q_i = q_i^{(0)} + Knq_i^{(1)} + Kn^2q_i^{(2)}\ldots \tag{14}$$

The zeroth order of this expansion leads to the Euler equation while the first one corresponds to the classical NSF theory. In this case, the Newton and Fourier laws, respectively, give the stress and heat flux vector for Maxwell gas:

$$\sigma_{ij}^{NFS} = -2\mu \frac{\partial v_{\langle i}}{\partial x_{j\rangle}}, \tag{15a}$$

$$q_i^{NFS} = -\frac{15}{4}\mu \frac{\partial \theta}{\partial x_i}. \tag{15b}$$

As in any problem involving partial differential equations, the solving of R13-moment equations requires a set of boundary conditions that one must specify. In this context, Torrilhon and Struchtrup have shown kinetically that $v_n, \sigma_{\tau n}, q_n, R_{\tau n}, m_{nnn}$, and $m_{\tau\tau n}$ are the only components that can be prescribed [30]. The subscripts τ and n denote the tangential and normal components of the tensors, respectively, where the wall normal is pointing toward the gas. Using the Maxwell accommodation model for boundary conditions results in a kinetic link between the moments in front of the wall and the tangential wall velocity v_τ^w and the wall temperature θ^w; the R13-BCs are written as

$$v_n = 0 \tag{16a}$$

$$\sigma_{\tau n} = -\chi/(2-\chi)\sqrt{\frac{2}{\pi\theta}}\left(\mathscr{P}\mathscr{V}_\tau + \frac{1}{5}q_\tau + \frac{1}{2}m_{\tau nn}\right), \tag{16b}$$

$$q_n = -\chi/(2-\chi)\sqrt{\frac{2}{\pi\theta}}\left(2\mathscr{P}\mathscr{T} - \frac{1}{2}\mathscr{P}\mathscr{V}_\tau^2 + \frac{1}{2}\theta\sigma_{nn} + \frac{1}{15}\Delta + \frac{5}{28}R_{nn}\right), \tag{16c}$$

$$R_{\tau n} = \chi/(2-\chi)\sqrt{\frac{2}{\pi\theta}}\left(6\mathscr{P}\mathscr{T}\mathscr{V}_\tau + \mathscr{P}\theta\mathscr{V}_\tau - \mathscr{P}\mathscr{V}_\tau^3 - \frac{11}{5}\theta q_\tau - \frac{1}{2}\theta m_{\tau nn}\right), \tag{16d}$$

$$m_{nnn} = \chi/(2-\chi)\sqrt{\frac{2}{\pi\theta}}\left(\frac{2}{5}\mathscr{P}\mathscr{T} - \frac{3}{5}\mathscr{P}\mathscr{V}_\tau^2 + \frac{7}{5}\theta\sigma_{nn} + \frac{1}{75}\Delta - \frac{1}{14}R_{nn}\right), \tag{16e}$$

$$m_{\tau\tau n} = -\chi/(2-\chi)\sqrt{\frac{2}{\pi\theta}}\left(\frac{1}{5}\mathscr{P}\mathscr{T} - \frac{4}{5}\mathscr{P}\mathscr{V}_\tau^2 + \frac{1}{14}R_{\tau\tau} + \theta\sigma_{\tau\tau} - (1/5)\theta\sigma_{nn} + \frac{1}{155}\Delta\right). \tag{16f}$$

Here $\mathscr{P} = \rho\theta + (1/2)\sigma_{\tau\tau} - (1/120)(\Delta/\theta) - (1/28)(R_{\tau\tau}/\theta)$.

Note that $\mathscr{V}_\tau = v_\tau - v_\tau^w$ and $\mathscr{T} = \theta - \theta^w$ represent, respectively, the velocity slip and temperature jump at the vicinity of the walls. The parameter χ is the Maxwell accommodation coefficient whose value is $\chi = 1$ for the full diffuse reflection and $\chi = 0$ for the specular one. The effect of such coefficient on thermal transpiration phenomena is evaluated using velocity dependent Maxwell (VDM) boundary condition and by means of DSMC method [31]. A heated microcavity with specular walls is also treated by means of NSF and moments theories [32, 33].

4. Numerical Scheme

To solve the above differential equations ((2a), (2b), (2c), (10), (11), (12a), (12b), and (12c)) in the steady state, it is more convenient to rewrite the equations in the condensed and matrix form:

$$A(\omega)\frac{\partial \omega}{\partial x} + B(\omega)\frac{\partial \omega}{\partial y} + \frac{1}{Kn}P(\omega)\omega = 0. \tag{17}$$

Here $\omega = [\rho, v_x, v_y, \theta, q_x, q_y, \sigma_{xx}, \sigma_{xy}, \sigma_{yy}, R_{xx}, R_{xy}, R_{yy}, m_{xxx}, m_{xxy}, m_{xyy}, m_{yyy}, \Delta]$ is the vector of field variables; $A(\omega)$, $B(\omega)$, and $P(\omega)$ are, respectively, the coefficient matrices in $x, y-$ directions and the production matrix. The matrix equation (17) is solved by means of finite difference approach. The cavity domain is discretized on a network of nodes in both directions. The R13 solution is obtained using the boundary conditions prescribed by a set of equations ((16a)–(16f)). In the slip flow regime, the Navier-Stokes and Fourier equations solution must be obtained with slip and jump boundary conditions. By ignoring the higher order term sm_{ijk}, R_{ik}, Δ and replacing the stress tensor and heat flux vector with their corresponding expressions of NSF, as indicated in the equations ((15a), (15b)), the first order of NSF-BCs can be written, therefore, as follows:

$$v_n = 0, \tag{18a}$$

$$\sigma_{\tau n}^{NSF(1)} = -\chi/(2-\chi)\sqrt{\frac{2}{\pi\theta}}\left(\mathscr{P}\mathscr{V}_\tau - \frac{3}{4}\mu\frac{\partial\theta}{\partial x_\tau}\right), \tag{18b}$$

$$q_n^{NSF(1)} = -\chi/(2-\chi)\sqrt{\frac{2}{\pi\theta}}\left(2\mathscr{P}\mathscr{T} - \frac{1}{2}\mathscr{P}\mathscr{V}_\tau^2 - \mu\theta\frac{\partial v_{\langle n}}{\partial x_{n\rangle}}\right), \tag{18c}$$

where $\mathscr{P} = \rho\theta + (1/2)\sigma_{\tau\tau}$.

Meanwhile, the second order of these BCs can be obtained using the second order of stress tensor and heat flux vector described by the Burnett equations [24, 34]:

$$v_n = 0, \tag{19a}$$

$$\sigma_{\tau n}^{NSF(2)} = -\chi/(2-\chi)\sqrt{\frac{2}{\pi\theta}}\left(\mathscr{P}\mathscr{V}_\tau + \frac{1}{5}q_\tau^{NSF} + \frac{m_{\tau nn}^{(2)}}{2} + \frac{1}{5}\frac{\mu^2}{\rho}\left(\frac{45}{16}\frac{\partial^2 v_\tau}{\partial x_k \partial x_k} - \frac{13}{4}\frac{\partial^2 v_k}{\partial x_k \partial x_\tau}\right)\right) - \frac{1}{18}\frac{R_{\tau n}^{(2)}}{\theta}, \tag{19b}$$

$$q_n^{NSF(2)} = -\chi/(2-\chi)\sqrt{\frac{2}{\pi\theta}}\left(2\mathscr{P}\mathscr{T} - \frac{1}{2}\mathscr{P}\mathscr{V}_\tau{}^2 + \frac{1}{2}\theta\sigma_{nn}^{NSF} + \frac{\Delta^{(2)}}{15} + \frac{13R_{mn}^{(2)}}{63}\right) - \frac{\mu^2}{\rho}\left(\frac{45}{16}\frac{\partial^2 v_n}{\partial x_k \partial x_k} - \frac{13}{4}\frac{\partial^2 v_k}{\partial x_k \partial x_n}\right), \quad (19c)$$

where the terms with the superscript $^{(2)}$ refer to the second order corrections which are obtained from the R13 constitutive relations (12a), (12b), and (12c) by replacing stress tensor and heat flux vector with their NSF expressions; these terms are given as follows:

$$R_{ij}^{(2)} = -\frac{24}{5}\frac{\mu}{\rho}\frac{\partial q_{\langle i}^{NSF}}{\partial x_{j\rangle}}, \quad (20a)$$

$$m_{ijk}^{(2)} = -2\frac{\mu}{\rho}\frac{\partial \sigma_{\langle ij}^{NSF}}{\partial x_{k\rangle}}, \quad (20b)$$

$$\Delta^{(2)} = -12\frac{\mu}{\rho}\frac{\partial q_k^{NSF}}{\partial x_k}. \quad (20c)$$

For more convenience, the results are shown with the dimensionless variables using the following normalizations:

$$x, y = x, \frac{y}{L},$$
$$V_i = \frac{v_i}{v_0},$$
$$q_i = \frac{q_i}{(\rho_0\theta_0 v_0)},$$
$$\overline{\rho} = \frac{\rho}{\rho_0},$$
$$\overline{\theta} = \frac{\theta}{\theta_0} \equiv \frac{T}{T_0}, \quad (21)$$
$$\overline{\sigma}_{ij} = \frac{\sigma_{ij}}{(\rho_0\theta_0)},$$
$$\overline{R}_{ij} = \frac{R_{ij}}{\left(\rho_0{\theta_0}^2\right)},$$
$$\overline{\Delta} = \frac{\Delta}{\left(\rho_0{\theta_0}^2\right)}$$
$$\text{and } \overline{m}_{ijk} = \frac{m_{ijk}}{(\rho_0\theta_0 v_0)}.$$

5. Results and Discussion

The behavior of gas flows in the slip and early transition regimes, often encountered in MEMS devices, is one of the challenging problems which need further investigations.

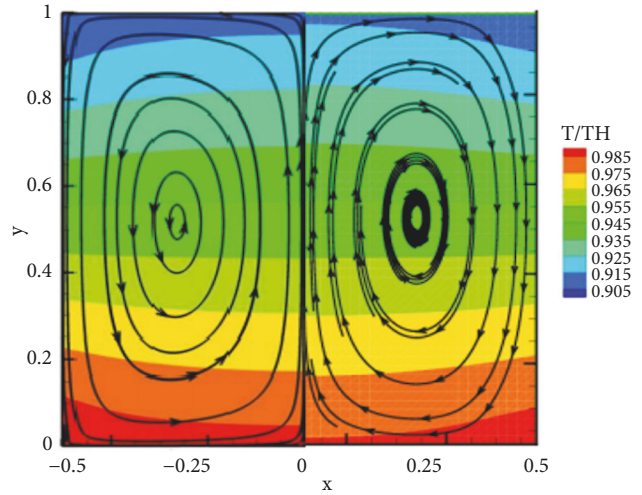

Figure 2: Streamlines and temperature contours comparison for $T_0/T_H = 0.9$ and $Kn = 0.1$ between R13 (right) and DSMC method [18] (left) adapted to the Vargas's problem (vertical, top-to-down, linearly heated cavity).

In this regime, the mean free path of gas is at the same order of or even much larger than the system characteristic length, the continuum assumption will break down, and the traditional CFD techniques will, therefore, lead to large errors [35]. The rarefaction effects influence the flow, such as heat flux induced by gradients of stresses even if there is no temperature gradient [36]. For validation purpose, firstly, we compare the DSMC and R13 results by considering the test case treated by Vargas et al. [18]. In this case, the gas flow is induced, on the one hand, by the thermal creep force created along the nonisothermal walls and, on the other hand, by a temperature gradient between the other walls. To stay in the considerations of macroscopic approaches, a small temperature gradient and moderate Knudsen number values are considered in this test case, $T_0/T_H = 0.9$, $Kn = 0.01$ and 0.1. In this case, the gas flow is subjected to two thermal forces: a *transpiration* force due to the linear profile imposed on the walls-temperature and *thermal stress* induced by the temperature gradient in bulk of flow. These forces may be acting in the same or opposite direction of the gas flow. Figure 2 shows the streamlines overlaid on the temperature contours obtained by both approaches.

R13 and DSMC predict two similar primary vortices in the flow field which push the flow from cold to hot region at the side walls. Kinetically, these patterns are interpreted by the fast motion of hot particles compared to particles coming from the colder region, which are slower. As a reaction, the wall is pushed toward the colder region, or, when the wall is at rest, the rarefied gas is driven from cold to hot, which is observed here. Both approaches give almost similar temperature distribution in the cavity.

In contrast with the classical problems of viscous flows induced by the relative motion of walls, this study focuses on the pure thermal creep flow induced only, in opposite directions, by the effects of nonisothermal walls as shown in Figure 1. To stay in the frame of small deviations from

equilibrium state, we restrict our attention to the macroscopic study of gas flow fields for a moderate temperature $T_H = 1.5T_0$ [37]. Then, we evaluate the effect of T_H on the maximum of tangential thermal-velocity along the bottom walls. By analogy with the viscous Couette flow [38, 39], the present problem of "thermal Couette flow" is treated by means of classical approach of NSF, with first and second orders of slip and jump BCs, and extended continuum theory.

The breakdown of the classical theory between the slip and transition regimes limit, $Kn = 0.1$, is clarified by solving the regularized 13-moment equations ($R13$). At low rarefaction degree, $Kn = 0.05$, the $R13$ approach predicts a primary vortex centered at $x = y = 0.5L$ while the $NSF(1)$ and $NSF(2)$ solutions envisage, inside this main vortex, two symmetric secondary vortices corresponding to the flow stagnation. Near longitudinal sides, the tangential temperature gradient forces a creep-driven flow in a circulatory motion from the cold to hot region. In addition to these eddies induced by the thermal convection phenomenon, thermal creep flow, two secondary symmetric counter-circulating vortices at the hot cavity corners are observed; see Figures 3(a), 3(c), and 3(e). The inverted transpiration force induced at the hot corners is the origin of these secondary vortices.

For $Kn = 0.3$, unlike first order solution which is not much sensitive to the rarefaction increase (Figure 3(b)), the second order solution (Figure 3(d)) predicts a little change in the center and size of vortices which correspond to the rarefaction effects contribution. In contrast to both NSF approaches, the $R13$ solution allows capturing the interplay between thermal stress and transpiration force, which are responsible for the streamlines inversion and disappearance observed at hot corners in the rarefied case. The third term in the $R13$-constitutive equation (10) expresses the thermal stress contribution. This is due to the predominance of nonequilibrium effects, with respect to thermal convection phenomenon, observed in the slightly rarefied case ($Kn = 0.05$). Indeed, the central vortex vanishes and the hot-corners vortices agglomerate to give an inverted circling of gas flow. This is in good agreement with the simplest *windmill* experiment realized by Sone [25] where the qualitative results are published through a brief communication [25] and recorded on a videotape (VHS). In this experiment, a rectangular glass plate of $70 \times 200\,mm$ was set in space with its longer sides in the vertical direction and electrically heated from the lower end of the plate (in back). A windmill was placed in front of the plate to detect the vertical flow induced by the heating process. The system is placed within a glass cylindrical chamber in which the pressure change is well controlled; the experimental protocol is shown in Figure 4. At the high-pressure condition, low rarefaction degree, the thermal convection phenomenon provides the windmill motion. This motion becomes increasingly slow with the pressure decrease. At low pressure, $\sim 40Pa$, the windmill motion is reversed by rarefaction effects. Experimentally, it fined as the pressure decreases; downward flow, a flow in the direction of the temperature gradient along the plate, grows and finally overcomes the thermal creep flow. This experiment was performed later with the same qualitative results in various systems with different windmills and plates.

The accuracy of the $R13$ solution, in the rarefied case, is also provided by a wide range of temperature variation, $1.04 \leq T/T_0 \leq 1.24$, unlike the closed one predicted by NSF solutions, especially the second order. The gas flow behavior is, therefore, influenced by both rarefaction and nonisothermal wall effects. To more understand this critical change, observed in the flow streamlines at the rarefied case (Figure 3(f)), the velocity and heat flux fields are evaluated in the vertical center-line; i.e., $x = L/2$. Figures 5 and 6 show the velocity and heat flux components as a function of $y-$coordinate. The rarefaction effects strongly influence the velocity fields, V_x and V_y. This higher sensitivity of velocity components is due to the small velocity-magnitude induced only by the longitudinal temperature gradient along the walls. Even at the slightly rarefied case, the classical NSF solutions cannot capture the nonlinear phenomenon contribution, which is more highlighted by solving the regularized 13-moment equations.

This velocity-rarefaction dependence is consistent with the experiment results for different pressure values. The combined effects of rarefaction and nonisothermal wall-driven is proved later by Sone through the improved version of his simple windmill experiment. The results show that the windmill rotation speed is strongly linked to the temperature gradient, i.e., the heating rate T_0/T_H, and the rarefaction degree (the pressure value in the chamber).

The $R13$ approach also provides a good clarification of the so-called Knudsen-layer which corresponds to the nonequilibrium area induced by the rarefaction effects near the heated walls, located at $y = 0, H$. The rarefaction effects also influence the profiles of heat flux components. At the slightly rarefied case, $Kn = 0.05$, the NSF approaches give rather similar profiles in the bulk region over the range of $0.25 \leq y/L \leq 0.75$. However, the validity of first and second orders BCs of NSF solution decreases with the increase of Knudsen number value before its breakdown for $Kn = 0.3$. Therefore, the enlargement of the Knudsen-layers in terms of Kn value, induced by the thermal creep flow, is more captured by the R13 solution, unlike the second order NSF2 which predicts only a small correction with respect to the first one NSF1.

This nonequilibrium region, which appears in the profiles of longitudinal components as a function of the normal coordinate, y, does not take place in the vertical ones. This is illustrated by the V_y and q_y profiles for $Kn = 0.05$ and 0.3 (Figure 6). With the second order of velocity slip and temperature jump BCs, the NSF theory predicts an improved correction of $y-$velocity and heat flux components in the rarefied case; see Figures 6(c) and 6(d). Figure 6 shows that the three solutions are almost confounded at the slightly rarefied case $Kn = 0.05$. However, for $Kn = 0.3$, the classical NSF theory, especially the first order one, cannot describe correctly the thermally driven rarefied gas flow behavior. Using the first order of slip and jump BCs, the slip velocity phenomenon is only induced in the proximity of walls, i.e., the Knudsen-layer, by the viscous slip flow. The sufficiency of this order of correction has been proved

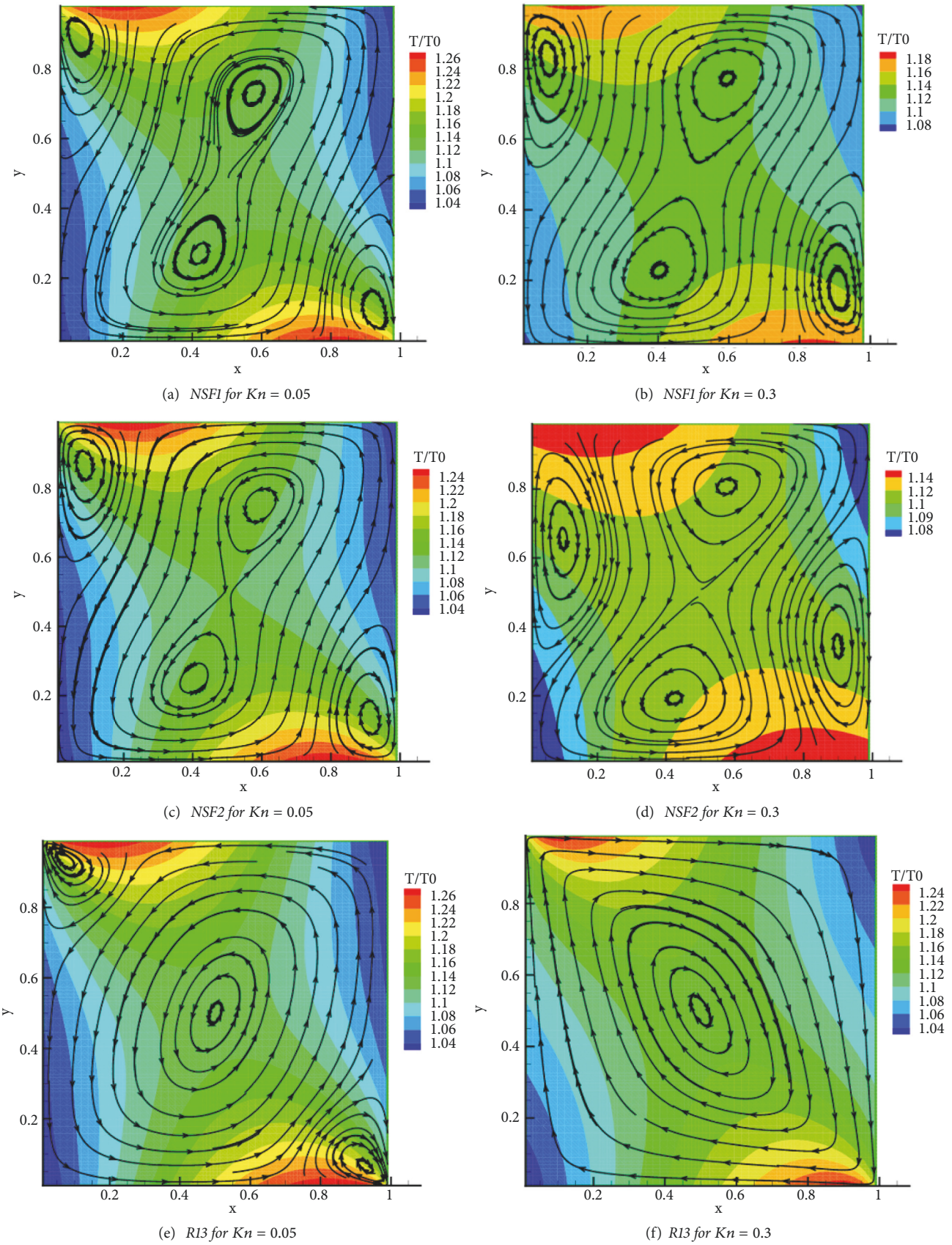

(a) *NSF1 for Kn* = 0.05

(b) *NSF1 for Kn* = 0.3

(c) *NSF2 for Kn* = 0.05

(d) *NSF2 for Kn* = 0.3

(e) *R13 for Kn* = 0.05

(f) *R13 for Kn* = 0.3

Figure 3: Streamlines overlaid on the temperature contours for $Kn = 0.05$ and 0.3 using NSF approaches (a-d) and R13 approach (e, f).

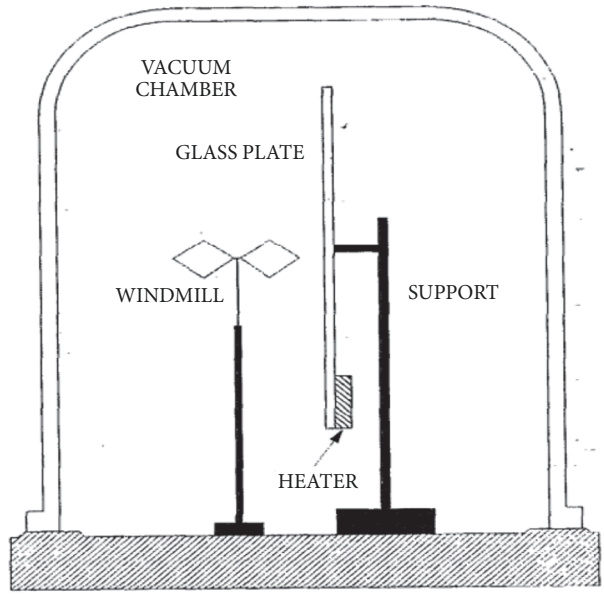

Figure 4: Windmill experimental apparatus [25].

recently by comparing the R13 results and those obtained by solving the linearized Boltzmann equation for viscous slip and transpiration flow problems [40, 41]. However, when the tangential temperature gradient is applied, i.e., $\partial T/\partial x_\tau \neq 0$, contribution of the second order term ($\sim Kn^2$) in the slip BCs must be considered. This explains the accuracy of NSF2 correction in the profile $V_x = f(y)$, with respect to the first one, NSF1.

To evaluate the combined effects of temperature gradient and rarefaction degree, we show the maximum value of V_x along the bottom wall as a function of Knudsen number for different temperatures, $1.25 \leq T_H/T_0 \leq 2$ (Figure 7). In conclusion, the maximum velocity along the wall depends on the gas flow regime defined by the Knudsen number value. In the slip regime, $Kn \leq 0.1$, $V_{x,max}$ decreases with the increase of rarefaction degree. After this limit, transition regime, the gas particles undergo a strong thermal motion at the wall proportional to Kn and T_H values.

To understand more about the heat transfer process induced by the temperature gradient, the heat-lines overlaid on the thermal shear stress contours obtained by NSF2 and R13 approaches are shown in Figure 8. Comparing the figures, one can conclude that both approaches provide a rather similar distribution of heat flux isolines at the slightly rarefied case ($Kn = 0.05$), while the longitudinal thermal stress magnitude is strongly influenced by the nonlinear mechanism of momentum transfer at the boundary. The nonlinear phenomena contribution, described with more details from the kinetic point of view, is well considered by the extended continuum theory of R13 by means of the terms R_{ij}, m_{ijk}, and Δ, unlike the NSF2 solution which gives a small range of change [41]. However, when the Knudsen number becomes larger ($Kn = 0.3$), the rarefaction effects influence the gas flow. The heat flux caused by the gradients of stresses and thermal creep is better described by R13 method [42, 43]. The rarefaction effect causes a change in the heat-lines curvature (Figure 9(d)), which is not predicted by NSF solution. This is due to the faster motion of particles coming from the hot corners than those coming from the cold ones. The stress quadratic flow, as well as nonlinear thermal stress effects, becomes larger in the flow bulk region [20].

The mutual interaction between the longitudinal walls, subject to the temperature gradient, on the flow pattern is evaluated by considering higher cavity ($H = 2L$), i.e., $AR = 2$. Figure 9 shows the streamlines superimposed on the temperature contours for $Kn = 0.05$ and 0.3 using both NSF1 and R13 approaches. Comparing these flow fields with the corresponding ones in the square case ($AR = 1$) in Figure 5, one can conclude that both solutions are sensitive to the cavity aspect ratio and rarefaction effects. For $Kn = 0.05$, the primary vortices observed between the cold corners in the square case, using NSF approach, are detached to form two secondary vortices on the side of lateral walls. However, at the rarefied case, the situation is reversed and the hot-corners vortices begin to agglomerate to form one primary vortex between the hot corners. However, the extended continuum method, R13, predicts rather similar fields but with small edges at the cold corners. For $Kn = 0.3$, two secondary vortices appear, under the vertical flow elongation effect, within the inverted vortex obtained between the hot corners in the square cavity case. These vortices are made to the flow stagnation appearing at $y = 0.5L$ and $1.5L$. On the other hand, the temperature contours show that the R13 approach predicts a larger range of temperature variation, T/T_0, in agreement with the rarefaction degree: [1.04 – 1.24] in square case and [1.02 – 1.22] for $AR = 2$. However, with the NSF solution, the temperature range varies from [1.08 – 1.18] to [1.065 – 1.13] in the higher cavity. The sensitivity of thermal

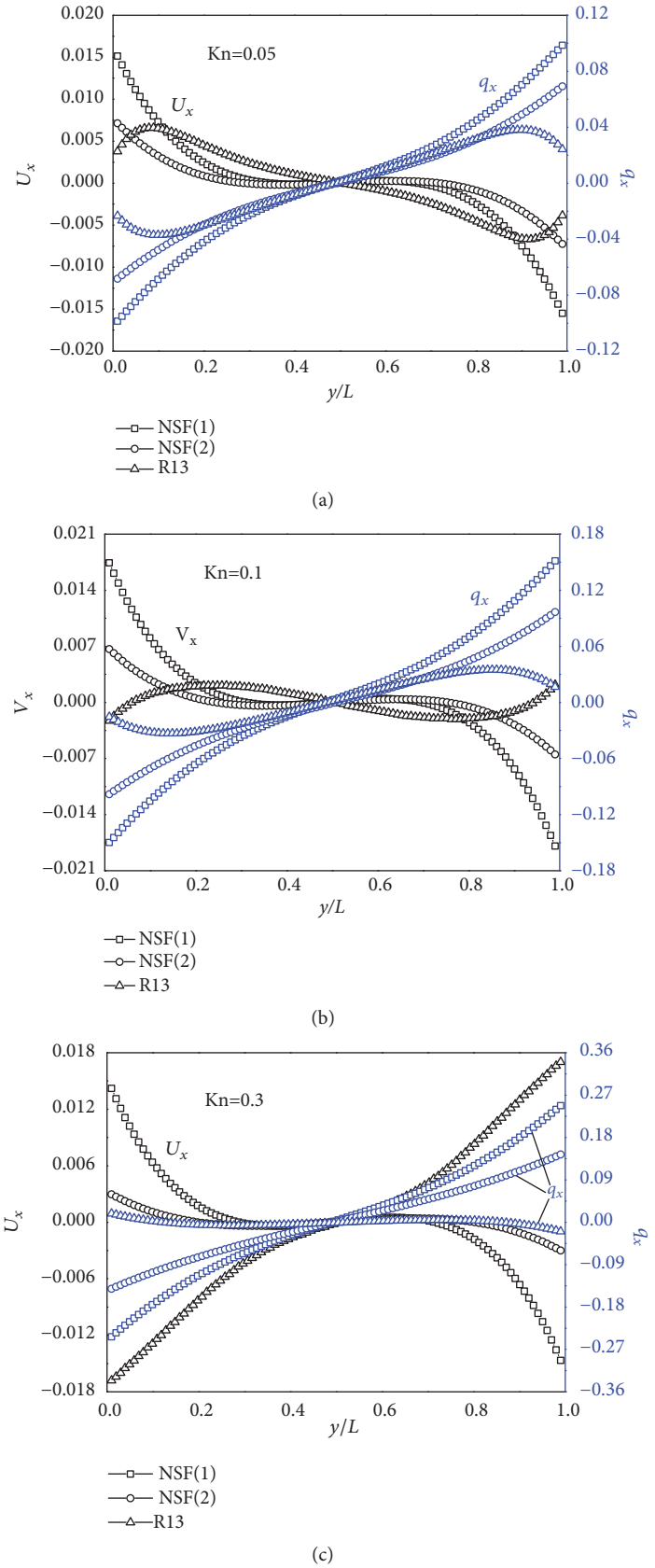

FIGURE 5: x–velocity and heat flux components profiles at the vertical center-line of the cavity for $Kn = 0.05$ (a), 0.1 (b), and 0.3 (c) using NSF1, NSF2, and R13 approaches; the black and blue symbols denote x–velocity and heat flux components, respectively.

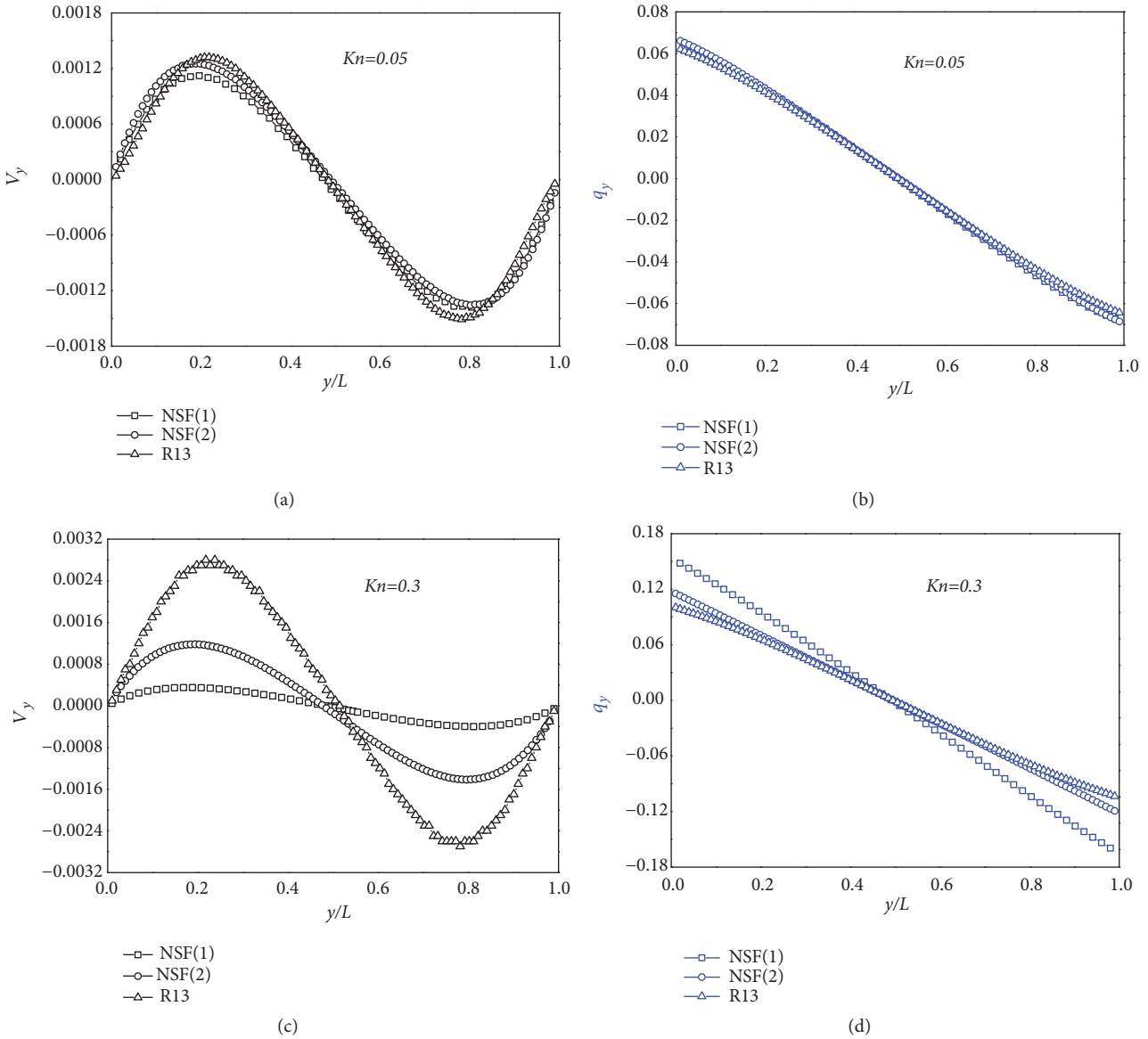

Figure 6: y−velocity and heat flux components profiles at the vertical center-line for $Kn = 0.05$ and 0.3 using NSF1, NSF2, and R13 approaches.

behavior with the cavity aspect ratio is, therefore, better captured by the extended continuum theory of R13 than by the classical one (NSF).

6. Concluding Remarks

In the present study, the behavior of a rarefied gas flow, induced thermally by nonisothermal wall effects within a microcavity, is investigated in the slip and early transition regimes. The problem is treated in the frame of classical and extended macroscopic theory by solving numerically, on the one hand, the Navier-Stokes and Fourier equations using the first and second orders of velocity slip and temperature jump and, on the other hand, the R13 set of equations. The gas flow sensitivity to the rarefaction degree is clarified using the main macroscopic flow fields. The results prove the break downs of NSF solutions at slip-transition regimes limit. Thus, the extended continuum solution allows the capture of the inverted motion of rarefied gas flow created by the thermal creep flow at the walls. This critical change in the flow streamlines is in a good agreement with the *windmill* experiment results realized by Sone. The nonlinear thermal stress and thermal creep co-contribution on the flow fields at the rarefied case have been illustrated by means of the R13 method. In view of different geometries that one can meet in several industrial applications, two different aspect ratios are evaluated in our study.

Data Availability

The data used to support the findings of this study are available from the corresponding author upon request.

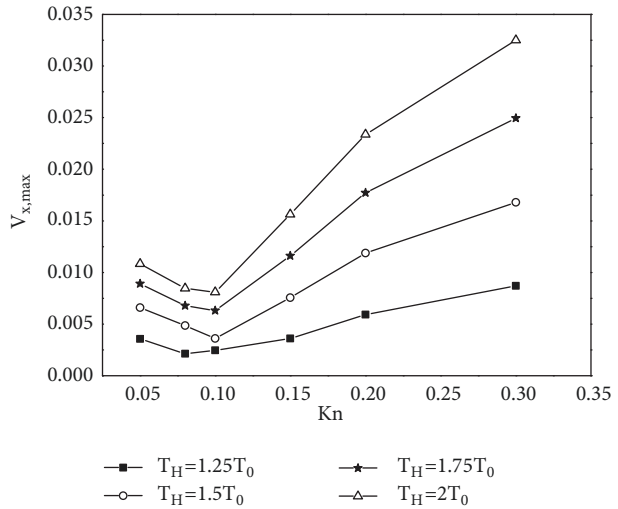

FIGURE 7: Maximum x–velocity along the bottom wall for different values of T_H.

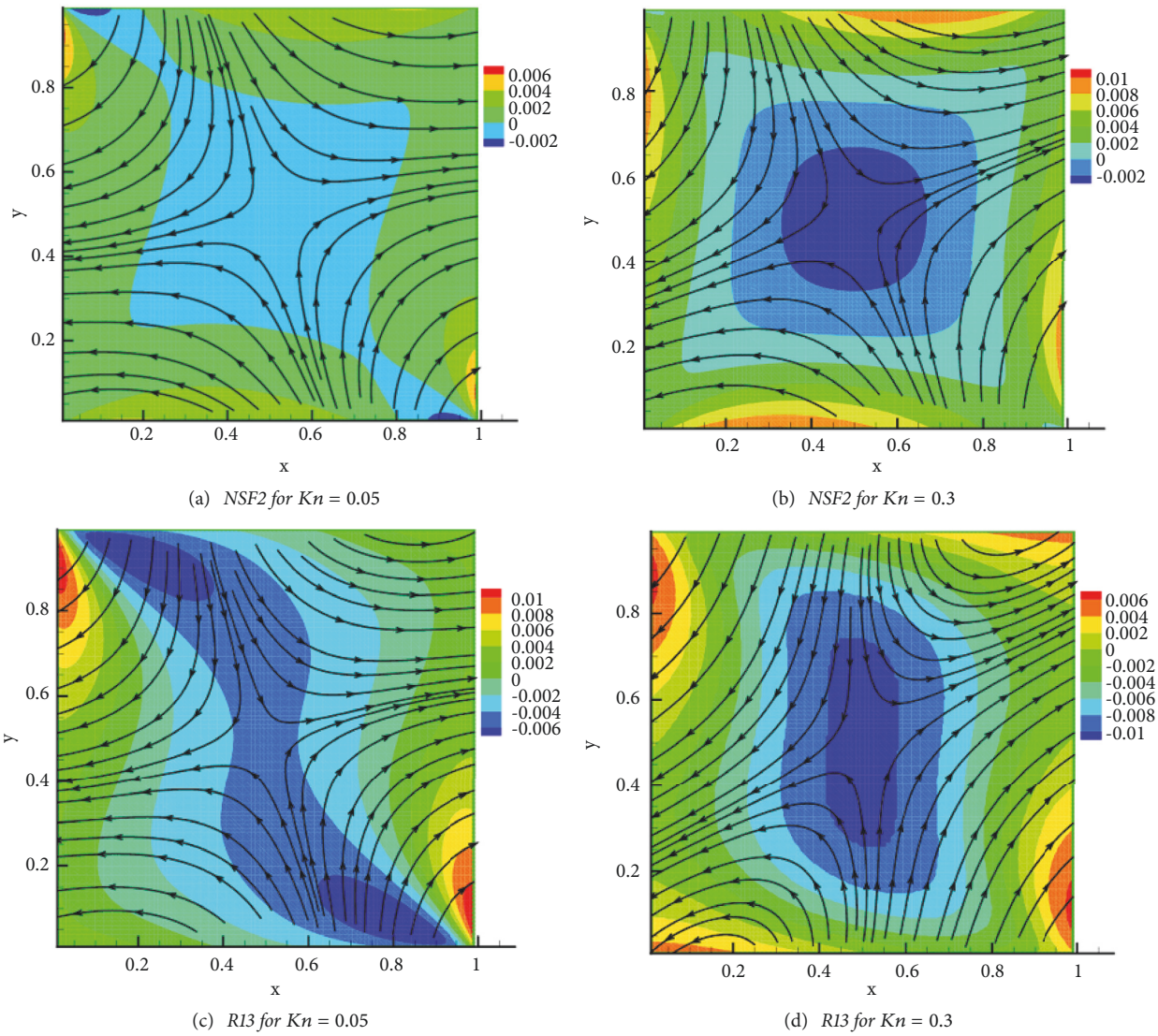

(a) *NSF2 for Kn* = 0.05

(b) *NSF2 for Kn* = 0.3

(c) *R13 for Kn* = 0.05

(d) *R13 for Kn* = 0.3

FIGURE 8: Heat-lines overlaid on the stress σ_{xy} contours for Kn = 0.05 and 0.3 using NSF2 (a, b) and R13 (c, d) approaches.

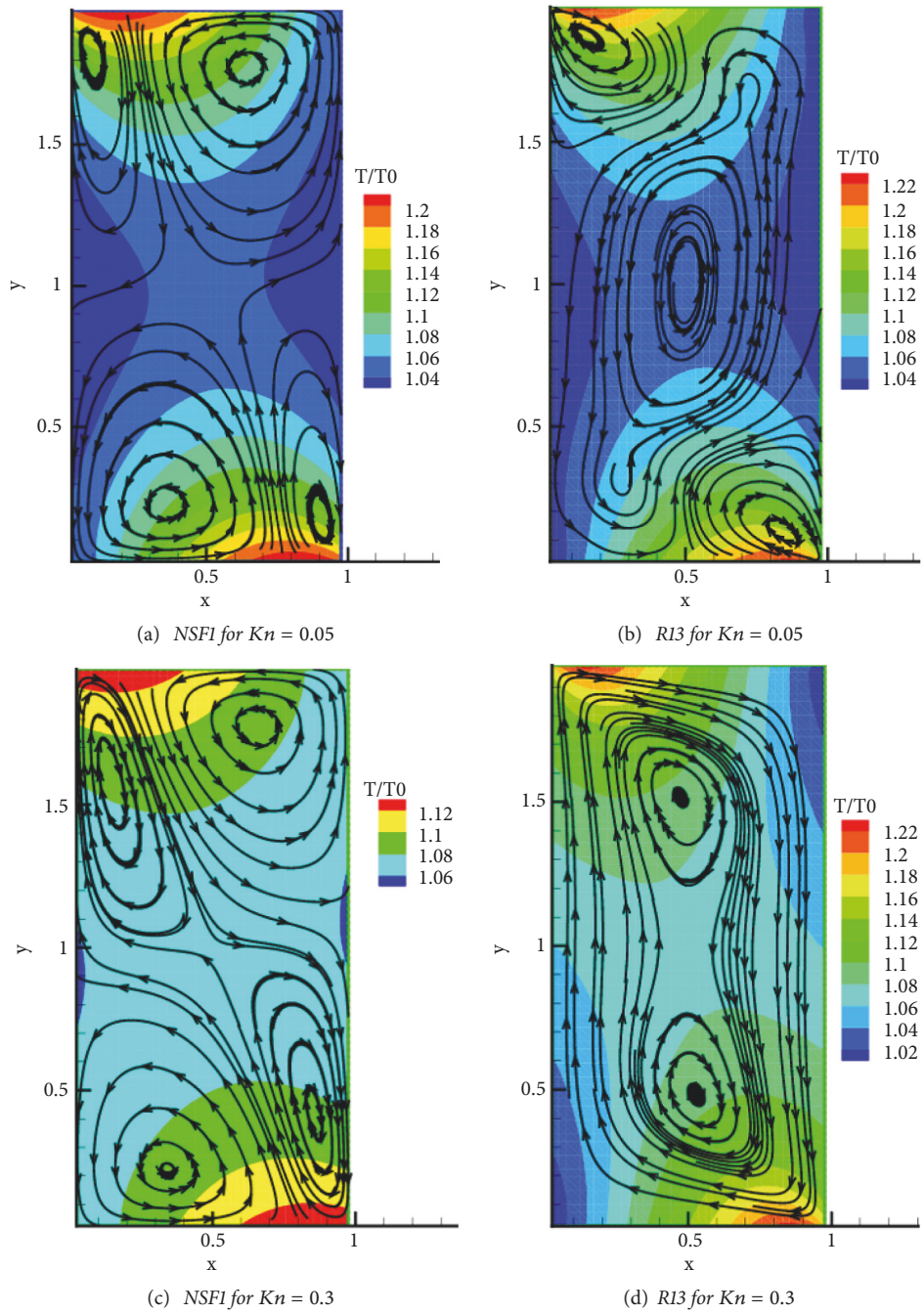

FIGURE 9: Streamlines overlaid on the temperature contours at $Kn = 0.05$ and 0.3 for $AR = 2$ using NSF1 and R13 approaches.

Conflicts of Interest

The authors declare that they have no conflicts of interest.

Acknowledgments

The authors gratefully acknowledge the valuable contribution of Mr. Vahid Shahabi, Member of the High Performance Computing (HPC) Laboratory, Department of Mechanical Engineering, Ferdowsi University of Mashhad, Mashhad, Iran, to the discussion of results and editing of the manuscript.

References

[1] I. A. Graur and A. P. Polikarpov, "Comparison of different kinetic models for the heat transfer problem," *Heat and Mass Transfer*, vol. 46, no. 2, pp. 237–244, 2009.

[2] H. A. Stone, A. D. Stroock, and A. Ajdari, "Engineering flows in small devices: microfluidics toward a lab-on-a-chip," *Annual Review of Fluid Mechanics*, vol. 36, pp. 381–411, 2004.

[3] H.-A. Yang, M. Wu, and W. Fang, "Localized induction heating solder bonding for wafer level MEMS packaging," *Journal of Micromechanics and Microengineering*, vol. 15, no. 2, pp. 394–399, 2005.

[4] W. Marques Jr., G. M. Kremer, and F. M. Sharipov, "Couette flow with slip and jump boundary conditions," *Continuum Mechanics and Thermodynamics*, vol. 12, no. 6, pp. 379–386, 2000.

[5] S. Mizzi, D. R. Emerson, S. K. Stefanov, R. W. Barber, and J. M. Reese, "Effects of rarefaction on cavity flow in the slip regime," *Journal of Computational and Theoretical Nanoscience*, vol. 4, no. 4, pp. 817–822, 2007.

[6] F. Sharipov, "Data on the velocity slip and temperature jump on a gas-solid interface," *Journal of Physical and Chemical Reference Data*, vol. 40, no. 2, Article ID 023101, pp. 1–28, 2011.

[7] A. Beskok and G. E. Karniadakis, "Simulation of heat and momentum transfer in complex microgeometries," *Journal of Thermophysics and Heat Transfer*, vol. 8, no. 4, pp. 647–655, 1994.

[8] E. Roohi, *DSMC Simulations of Nanoscale and Microscale Gas Flow, Encyclopedia of Microfluidics and Nanofluidics*, Springer Science+Business Media, New York, NY, USA, 2013.

[9] E. Roohi, M. Darbandi, and V. Mirjalili, "DSMC Solution of Subsonic Flow through Micro-Nano Scale Channels," *Journal of Heat Transfer*, vol. 131, no. 9, p. 092402, 2009.

[10] J. Fan and C. Shen, "Statistical simulation of low-speed rarefied gas flows," *Journal of Computational Physics*, vol. 167, no. 2, pp. 393–412, 2001.

[11] E. Y. Moghadam, E. Roohi, and J. A. Esfahani, "Heat transfer and fluid characteristics of rarefied flow in thermal cavities," *Vacuum*, vol. 109, no. 1, pp. 333–340, 2014.

[12] F. Sharipov and V. Seleznev, "Data on internal rarefied gas flows," *Journal of Physical and Chemical Reference Data*, vol. 27, no. 3, pp. 657–706, 1998.

[13] F. Sharipov, "Application of the Cercignani-Lampis scattering kernel to calculations of rarefied gas flows. I. Plane flow between two parallel plates," *European Journal of Mechanics - B/Fluids*, vol. 21, no. 1, pp. 113–123, 2002.

[14] R. D. Garcia and C. E. Siewert, "The linearized Boltzmann equation with Cercignani–Lampis boundary conditions: Basic flow problems in a plane channel," *European Journal of Mechanics - B/Fluids*, vol. 28, no. 3, pp. 387–396, 2009.

[15] A. Rana, M. Torrilhon, and H. Struchtrup, "Heat transfer in micro devices packaged in partial vacuum," *Journal of Physics: Conference Series*, vol. 362, no. 1, Article ID 012034, 2012.

[16] L. Zhu, S. Chen, and Z. Guo, "dugksFoam: An open source OpenFOAM solver for the Boltzmann model equation," *Computer Physics Communications*, vol. 213, pp. 155–164, 2017.

[17] S. Kosuge, K. Aoki, S. Takata, R. Hattori, and D. Sakai, "Steady flows of a highly rarefied gas induced by nonuniform wall temperature," *Physics of Fluids*, vol. 23, no. 3, Article ID 030603, 2011.

[18] M. Vargas, G. Tatsios, D. Valougeorgis, and S. Stefanov, "Rarefied gas flow in a rectangular enclosure induced by non-isothermal walls," *Physics of Fluids*, vol. 26, no. 5, Article ID 057101, 2014.

[19] A. Mohammadzadeh, A. S. Rana, and H. Struchtrup, "Thermal stress vs. thermal transpiration: A competition in thermally driven cavity flows," *Physics of Fluids*, vol. 27, no. 11, Article ID 112001, 2015.

[20] Y. Sone, *Molecular Gas Dynamics: Theory, Techniques, and Applications*, Springer Science & Business Media, 2007.

[21] F. Sharipov, *Rarefied Gas Dynamics: Fundamentals for Research and Practice*, Wiley-VCH, 2016.

[22] G. C. Birur, S. T. Waniewski, A. D. Paris, P. Shakkottai, and A. A. Green, "Micro/nano spacecraft thermal control using a MEMS-based pumped liquid cooling system," in *Proceedings of the Micromachining and Microfabrication, International Society for Optics and Photonics*, pp. 196–206, 2001.

[23] A. S. Rana, A. Mohammadzadeh, and H. Struchtrup, "A numerical study of the heat transfer through a rarefied gas confined in a microcavity," *Continuum Mechanics and Thermodynamics*, vol. 27, no. 3, pp. 433–446, 2015.

[24] H. Struchtrup, *Macroscopic Transport Equations for Rarefied Gas Flows*, Springer, New York, 2005.

[25] Y. Sone, "A simple demonstration of a rarefied gas flow induced over a plane wall with a temperature gradient," *Physics of Fluids*, vol. 3, no. 5, pp. 997-998, 1991.

[26] H. Grad, *Physica A: Statistical Mechanics and its Applications*, Mimeographed notes, New York University, 1949.

[27] H. Struchtrup and M. Torrilhon, "Regularization of Grad's 13 moment equations: derivation and linear analysis," *Physics of Fluids*, vol. 15, no. 9, pp. 2668–2680, 2003.

[28] S. Mizzi, X. J. Gu, D. R. Emerson, R. W. Barber, and J. M. Reese, "Computational framework for the regularized 20-moment equations for non-equilibrium gas flows," *International Journal for Numerical Methods in Fluids*, vol. 56, no. 8, pp. 1433–1439, 2008.

[29] A. Rana, M. Torrilhon, and H. Struchtrup, "A robust numerical method for the R13 equations of rarefied gas dynamics: application to lid driven cavity," *Journal of Computational Physics*, vol. 236, no. 1, pp. 169–186, 2013.

[30] M. Torrilhon and H. Struchtrup, "Boundary conditions for regularized 13-moment equations for micro-channel flows," *Journal of Computational Physics*, vol. 227, no. 3, pp. 1982–2011, 2008.

[31] A. Mohammadzadeh and H. Struchtrup, "Velocity dependent Maxwell boundary conditions in DSMC," *International Journal of Heat and Mass Transfer*, vol. 87, pp. 151–160, 2015.

[32] J. Baliti, M. Hssikou, and M. Alaoui, "The 13-moments method for heat transfer in gas microflows," *Australian Journal of Mechanical Engineering*, pp. 1–14, 2017.

[33] J. Baliti, M. Hssikou, and M. Alaoui, "Numerical simulation of heat transfer in a micro-cavity," *Canadian Journal of Physics*, vol. 95, no. 1, pp. 85–94, 2016.

[34] M. Torrilhon and H. Struchtrup, "Regularized 13-moment equations: shock structure calculations and comparison to Burnett models," *Journal of Fluid Mechanics*, vol. 513, pp. 171–198, 2004.

[35] G. Karniadakis, A. Beskok, and N. Aluru, *Micro Flows: Fundamentals and Simulation*, Springer, 2005.

[36] M. N. Kogan, V. S. Galkin, and O. G. Fridlender, "Stresses produced in gasses by temperature and concentration inhomogeneities. New types of free convection," *Soviet Physics Uspekhi*, vol. 19, no. 5, pp. 420–428, 1976.

[37] D. H. Papadopoulos and D. E. Rosner, "Enclosure gas flows driven by non-isothermal walls," *Physics of Fluids*, vol. 7, no. 11, pp. 2535–2537, 1995.

[38] M. Hssikou, J. Baliti, and M. Alaoui, "Extended macroscopic study of dilute gas flow within a microcavity," *Modelling and Simulation in Engineering*, vol. 2016, Article ID 7619746, 9 pages, 2016.

[39] M. Hssikou, J. Baliti, and M. Alaoui, "The planar Couette flow with slip and jump boundary conditions in a microchannel," *Monte Carlo Methods and Applications*, vol. 22, no. 4, pp. 337–347, 2016.

[40] A. S. Rana and H. Struchtrup, "Thermodynamically admissible boundary conditions for the regularized 13 moment (R13) equations," *Physics of Fluids*, vol. 28, Article ID 027105, 2016.

[41] T. Ohwada, Y. Sone, and K. Aoki, "Numerical analysis of the shear and thermal creep flows of a rarefied gas over a plane wall on the basis of the linearized Boltzmann equation for hardsphere molecules," *Physics of Fluids A. Fluid Dynamics*, vol. 1, pp. 1588–1599, 1989.

[42] A. V. Bobylev, "Quasistationary hydrodynamics for the Boltzmann equation," *Journal of Statistical Physics*, vol. 80, no. 5-6, pp. 1063–1083, 1995.

[43] E. Yariv, "Thermophoresis due to strong temperature gradients," *SIAM Journal on Applied Mathematics*, vol. 69, no. 2, pp. 453–472, 2008.